Journal of Electrochemical Science and Technology
Vol. 3, No. 3, 2012, 116-122
http://dx.doi.org/10.5229/JECST.2012.3.3.116

Journal of Electrochemical Science and Technology

A Carbon Nanotubes-Silicon Nanoparticles Network for High Performance Lithium Rechargeable Battery Anodes

Byung Gon Kim[a], Weon Ho Shin[a], Soo Yeon Lim[a], Byung Seon Kong[b], and Jang Wook Choi[a,†]
[a]*Graduate School of EEWS (WCU) and KAIST Institute NanoCentury, Korea Advanced Institute of Science and Technology (KAIST), 373-1 Guseong-dong, Yuseong-gu, Daejeon 305-701, Korea*
[b]*KCC Central Research Institute, 83, Mabook Dong, Giheung Gu, Yongin-Si, Gyunggi-Do 446-912, Korea*

ABSTRACT :

As an effort to address the chronic capacity fading of Si anodes and thus achieve their robust cycling performance, herein, we develop a unique electrode in which silicon nanoparticles are embedded in the carbon nanotubes network. Utilizing robust contacts between silicon nanoparticles and carbon nanotubes, the composite electrodes exhibit excellent electrochemical performance : 95.5% capacity retention after 140 cycles as well as rate capability such that at the C-rate increase from 0.1C to 1C to 10C, the specific capacities of 850, 698, and 312 mAh/g are obtained, respectively. The present investigation suggests a useful design principle for silicon as well as other high capacity alloying electrodes that undergo large volume expansions during battery operations.

Keywords : Silicon, Carbon nanotube, Chemical vapor deposition, Lithium ion battery, Anode.

Received August 22, 2012 : Accepted September 30, 2012

1. Introduction

As the demand on lithium ion batteries (LIBs) with high energy densities is rapidly increasing to enable emerging large-scale applications such as electrical vehicles and stationary grid storage systems,[1,2] silicon (Si) is receiving considerable attention due to its unparalleled capacity (> 3,000 mAh/g), which is significantly larger than those of conventional graphite electrodes.[3,4] Despite the superior specific capacity, Si suffers from insufficient cycle life, which has been known to originate from large volume changes of Si during repeated charge and discharge. The large volume change causes fast capacity decay by triggering various fading mechanisms such as pulverization, contact loss with conducting agents, and unstable solid-electrolyte-interphase (SEI) formation.[3,5] Extensive studies have revealed that the pulverization issue can be avoided by scaling-down the sizes of active materials, and along this direction diverse nanostructured Si electrodes including nanoparticles,[6-9] nanowires,[5,10-13] nanotubes,[14-16] and porous structures demonstrated substantially improved cycle life.[17,18] Although these nanostructures have exhibited promising electrochemical performances, nanoparticles composited with carbon materials might be one of the most viable options for large-scale production.[19-22] Other morphologies require relatively more complicated or more expensive synthetic procedures which might not be acceptable in large quantity production.

Having noticed that Si-carbon composites could also alleviate the contact loss with conducting agent,[19-24] in the present study, we develop a composite structure consisting of Si nanoparticles (NPs) and carbon nanotubes (CNTs). In particular, as an effort to develop an organized structure, CNTs were grown via a chemical vapor deposition (CVD) process to homogenously surround Si NPs and thus to ensure robust contacts between both components. The CNT network contrib-

†Corresponding author. Tel.: +82-42-350-1719
E-mail address: jangwookchoi@kaist.ac.kr

utes to good electric conduction throughout the entire electrode film. After an optimization of the Si:C ratio, the network composite shows excellent electrochemical results: the specific capacity after 140 cycles is 601.5 mAh/g based on the total weight of the SiNP-CNT composite, which corresponds to 95.5% capacity retention with respect to its initial capacity. The coulombic efficiency also reaches 99.3% at a 0.5 C rate (1 C: each of charge and discharge takes 1 h). The present investigation suggests that highly organized CNTs network integrated with Si NPs is a robust platform suitable for high performance LIB anodes.

2. Experiment

2.1. Preparation of SiNP-CNT composite

Si NPs were donated from KCC, Korea and were used as received. 10 mg Si NPs were dispersed in 50 mL ethylene glycol (Junsei, Japan) by stirring at 120°C. In order to homogenously attach iron (Fe) particle catalysts onto the Si NP solution, iron (II) acetate (Aldrich, USA) was first dissolved in the Si NPs dispersion. Then, $NaBH_4$ (Aldrich, USA) was added to the dispersion to reduce iron (II) acetate. After 2 hrs of the reduction reaction at 120°C, the solution was cooled down to room temperature. Next, the product, a mixture of Si NPs and Fe NPs, was acquired by filtration and was washed 3 times with acetone. By varying the Fe precursor concentration, the samples with 10, 22, and 34 wt% of Fe were prepared.

The subsequent CNTs growth was carried out by a CVD process using a tube-type furnace. For the growth, the Si-Fe samples were first heated to 500°C under an Ar flow (200 sccm) and the tube pressure was set to 85 torr. The Ar was fed into the tube to prevent oxidation at high temperature. Then, the furnace was heated further to 700°C under a flow of H_2 gas (200 sccm) at the same pressure. Finally, CNTs were grown by feeding a mixture gas of C_2H_2 (15 sccm), Ar (70 sccm), and H_2 (30 sccm) under a pressure of 65 torr for 30 min while the temperature was maintained at 700°C. Once the growth is completed, the SiNP-CNT composite was cooled down to room temperature under an Ar atmosphere.

2.2. Electrochemical test

In order to evaluate electrochemical performance, the SiNP-CNT electrodes were prepared on copper foil (18 um thickness, Hohsen, Japan). The SiNP-CNT composite was first mixed with Super P (TIMCAL, Switzerland) and poly(acrylic acid) (PAA, M_w = 3,000,000, Aldrich, USA) at a weight ratio of 8 (active material): 1 (Super P): 1 (binder) and were then dissolved in 1-Methyl-2-pyrrolidinone (NMP, Aldrich, USA) to form a homogeneous slurry. The slurry was cast onto a copper foil using the doctor blade method and was dried overnight at 383 K in a vacuum oven. The 2032 coin-type half-cells were assembled using lithium metal foil as the counter/reference electrodes and Celgard 2400 film as separators in a glove box with < 20 ppm oxygen. The electrolyte was 1 M $LiPF_6$ in 1:1 w/w mixture of ethylene carbonate (EC) and diethyl carbonate (DEC) (PANAX E-TEC, Korea) with vinylene carbonate (3 wt%, PANAX E-TEC, Korea). The galvanostatic charge and discharge tests were conducted by using a WBCS 3000 battery cycler (Wonatech, Korea) by adopting cut-off voltages at 0.005 and 1.5 V (vs. Li/Li^+).

2.3. Materials characterization

The crystal structures of the bare Si NPs and SiNP-CNT composites were characterized by X-ray diffraction (micro XRD, Rigaku) with Cu K_α (λ = 0.15406 nm). Field emission scanning electron microscope (FE-SEM, Sirion) was employed to investigate the morphologies of the bare Si NPs and SiNP-CNT composites. The dispersion of Fe NPs in the Si NPs clusters was characterized using field emission transmission electron microscopy (FE-TEM, TECNAI) and Fourier transformed (FT) pattern. The elemental analysis and mapping of the samples were conducted using an energy-dispersive X-ray spectroscopy (EDAX). In order to identify the exact Si weight portion in the network composite, inductively coupled plasma (ICP, Spectro) and thermogravimetric analysis (TGA, Netzsch) were performed. During the TGA analysis, the heating rate was set to 10°C/min under an air flow.

3. Results and discussion

3.1. The characterization of SiNP-CNT composites

As mentioned above, in order to grow CNTs around Si NPs, Fe NPs were first attached onto the surfaces of Si NPs during the chemical reduction process to serve as catalysts. ICP analyses indicate that the Fe/Si weight ratios for the three cases prepared are 10, 22, and 34 wt% (Table 1). The attachment of Fe NPs on

Table 1. ICP data indicative of the Fe/Si ratio

	Si NPs	Fe NPs	Ratio (Fe/Si)
Si + Fe 10 wt%	88.777	8.8369	0.09954
Si + Fe 22 wt%	56.309	12.456	0.22120
Si + Fe 34 wt%	47.868	16.552	0.34578

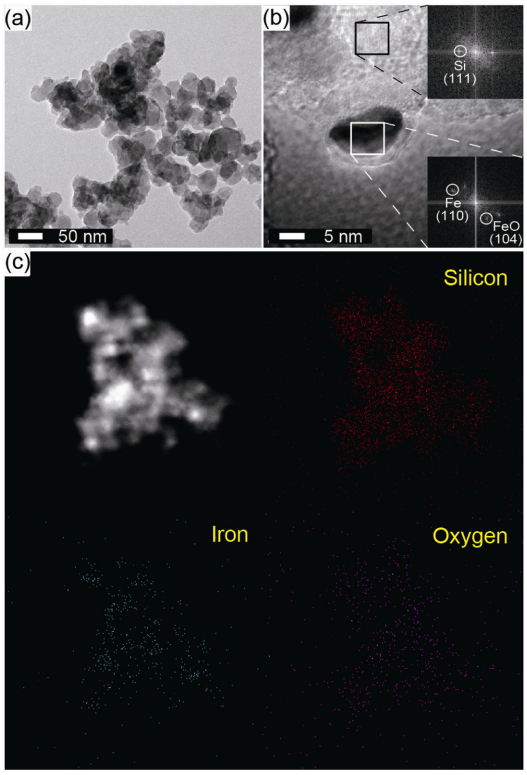

Fig. 1. Characterization of catalytic Fe NPs in the Si NPs cluster. TEM images of the sample at (a) low and (b) high magnifications. (b, inset) FT patterns obtained from the black (Si) and white (Fe and FeO) boxes in (b). (c) A scanning transmission electron microscopy (STEM) image of the sample (top-left) alongside EDAX elemental mappings for silicon, iron, and oxygen.

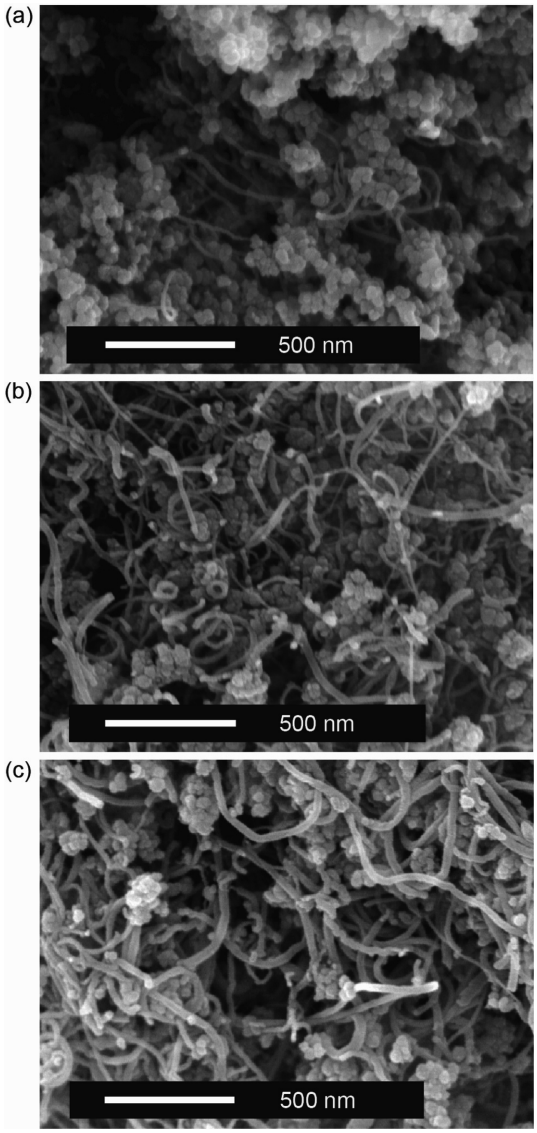

Fig. 2. SEM images of the SiNP@CNT composites based on different Fe/Si weight ratios. The corresponding Fe contents are (a) 10 wt%, (b) 22 wt%, and (c) 34 wt%.

the Si NPs was confirmed by TEM analyses. As shown in Fig. 1(a) at a low magnification, it appears that Fe NPs (darker spots) around ~10 nm are attached on the Si NPs whose diameters are 40~80 nm. A TEM image at a higher magnification provides a more direct evidence of Fe NPs on Si NPs (Fig. 1(b)). The FT patterns taken from the black and white boxes exhibit diffraction spots corresponding to the (111) plane of Si (black box), the (110) plane of Fe, and the (104) plane of FeO (white box) (Fig. 1(b) inset). Also, EDAX elemental mapping of the NP clusters verifies further the well-dispersed Fe catalysts on the Si NPs (Fig. 1(c)). The Fe elemental signal matches well with the Si signal over the cluster.

Fig. 2 shows the SiNP-CNT composites based on different Fe/Si ratios in the Fe weight content range of 10~34%. While all of samples show Si NPs uniformly embedded in the CNT networks, which should originate from the uniformly distributed Fe catalysts in the

pre-growth stage, the images over multiple spots are likely to show a trend that Si NPs appear less frequently in the samples with higher Fe/Si values. This trend implies that the Si/C ratio in the final sample can be tuned by the initial catalyst concentration. Such capability was verified directly by TGA results in Fig. 3(a): The Fe weight contents of 10, 22, and 34% result in the carbon weight contents of 7.5, 21.6 and 40.4% in the final SiNP-CNT composites. In addition, XRD characterization was performed (Fig. 3(b)) to identify the components and crystal structures of SiNP-CNT composites. While the XRD peaks confirm the presence of Si, C, and Fe, the data also indicate the formation of impurity phases of Fe_3C and $FeSi_2$. The formation of Fe_3C has been reported for the cases that carbon containing gases such as C_2H_2 and CH_4 react with Fe elements in the reduction atmosphere.[25,26] For the case of $FeSi_2$, it has been known that Si can form alloys with Fe along the interface of both components during high temperature processes near 700°C.[5] However, $FeSi_2$ was found not to react with Li ions during electrochemical cycling.[27]

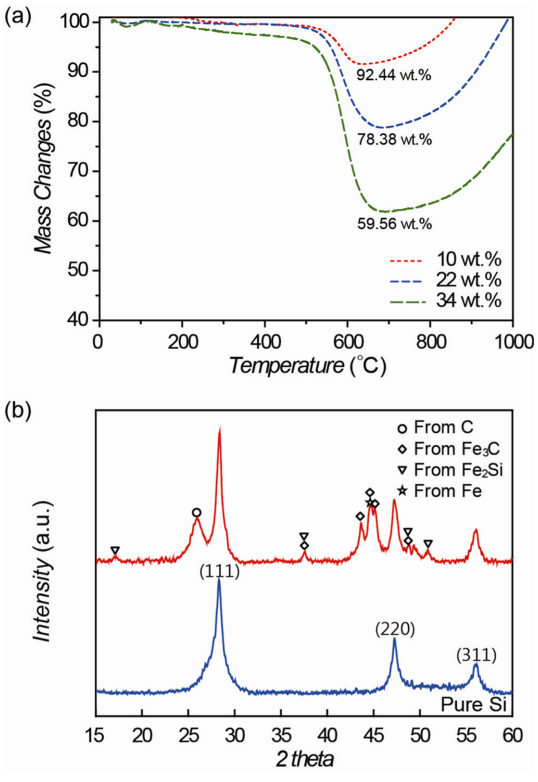

Fig. 3. (a) TGA results of the samples with various Fe contents. (b) XRD patterns of bare Si NPs (lower line) and the SiNP@CNT composite based on 34 wt% of Fe content (upper line).

3.2. Electrochemical analysis

Fig. 4(a) shows cyclic voltammetry (CV) curves at the 2nd, 20th, and 50th cycles for the 34 wt% SiNP-CNT case in the potential window of 0.005~1.5 V measured at a scan rate of 1 mV/s. The observed two peaks at

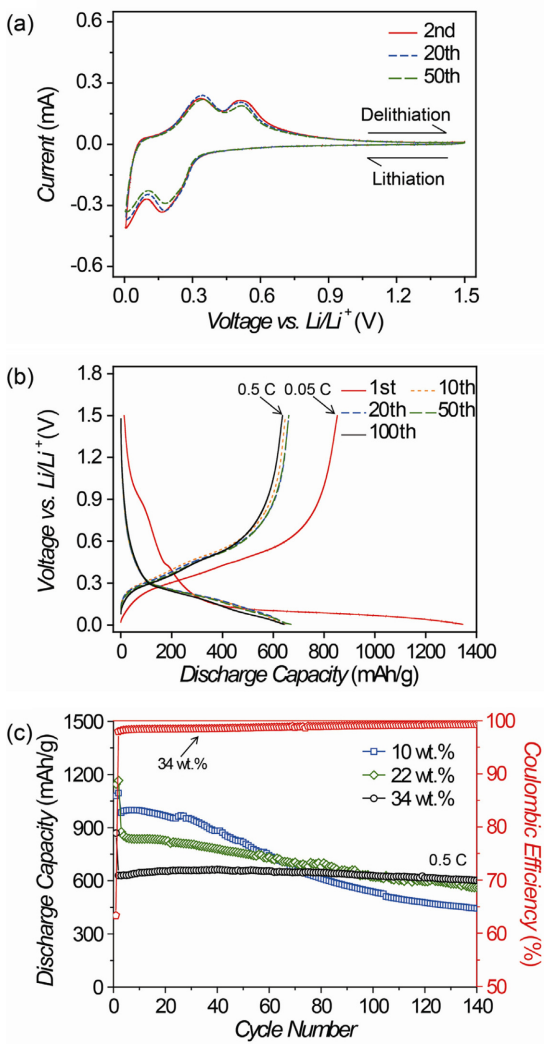

Fig. 4. Electrochemical data for the SiNP@CNTs composites. (a) CV curves of the 34 wt% sample measured at 1 mV/s in the range of 0.005~1.5 V versus Li/LI^+. (b) Voltage profiles of the 34 wt% sample at different cycle numbers. (c) Cycling performance of the samples based on different Fe contents.

0.18 and 0.01 V during lithiation as well as 0.34 and 0.51 V during delithiation are indicative of Si reactions with Li and are indeed consistent with previously reported values.[5,28] The magnitudes of these peaks are maintained for 50 cycles, suggesting robust electrochemical cycling originating from structural stability of the SiNP-CNT composite. The potential profiles of the 34 wt% SiNP-CNT composite are displayed in Fig. 4(b). In these measurements, the first 2 cycles were measured at 0.05 C and the C-rate was increased to 0.5 C thereafter. The charge (lithiation) plateau at ~0.8 V in the first cycle is ascribed to the SEI layer formation.[29,30] The plateau locations during both lithiation and delithiation are also consistent with the aforementioned CV data as well as previously reported values. The Coulombic efficiency in the first cycle turns out to be 63%. The relatively low Coulombic efficiency must be associated with the SEI formation over the large surface area of the SiNP-CNT composite.[6,7]

Cycle performance displayed in Fig. 4(c) exhibits the dependence of the Fe/Si weight ratio. Although all of these measurements were done consistently at 0.5 C, the 10 and 22 wt% cases show gradual decay in the capacity during cycling, whereas the 34 wt% case shows far superior capacity retention: the 10 and 22 wt% cases retain only 45 and 64.2% of the initial capacities after 140 cycles, respectively. By contrast, the 34 wt% case retains 95.5% after the same number of cycles. Due to the smaller Si weight portion, the initial specific capacity of the 34 wt% case is smaller than those of the other two cases: The 10, 22, and 34 wt% cases exhibit initial capacities of 984, 875, and 630 mAh/g, respectively. These results suggest that certain amounts of CNTs are required to preserve initial capacities perhaps because sufficient CNT network is necessary to guarantee robust contacts between Si NPs and CNTs during repeated volume changes of Si NPs. Moreover, it is noteworthy that the 34 wt% composite gradually increases its coulombic efficiency and its values reach 99.3% after 140 cycles. The coulombic efficiency was preserved throughout the remaining cycles. The excellent coulombic efficiencies are ascribed to the robust structure of the composite that maintains SEI layers in a stable manner.

In order to evaluate the rate capability of the SiNP-CNT composites, the 34 wt% case was tested at different C-rates (Fig. 5). The SiNP-CNT composite shows outstanding rate capability: when the C-rate increases

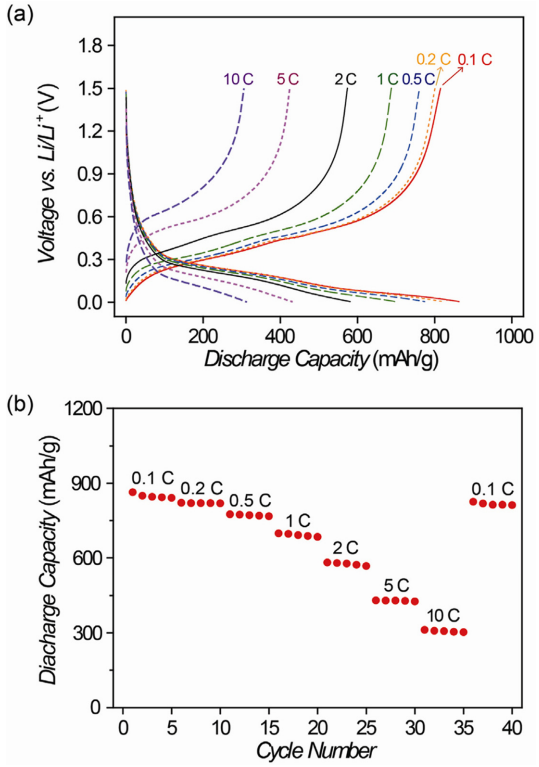

Fig. 5. (a) Voltage profiles of the 34 wt% sample at different C-rates. (b) A summarized result of the rate capability for the 34 wt% sample.

from 0.1 C to 1 C to 10 C, its capacities are changed from 850 to 698 to 312 mAh/g, respectively, implying that even under a 100-fold current increase, 36.7% of the original capacity is still preserved. Such superb rate capability is attributed to the CNTs network that enables efficient electronic diffusion through the network while Li ions freely diffuse through the void spaces between CNTs.

The structural stability of the SiNP-CNT composite was verified by SEM images taken after 100 cycles (Fig. 6). Unlike the reported Si nanostructures that suffer from the fracture and film delamination after many cycles,[31,32] the SEM images indicate that the overall morphology of the electrode is well-maintained compared to the pristine electrode (Fig. 6(a) and (b)) although some of Si NPs are not clearly visible due to the SEI layers. The SEM images confirm again that the CNTs network acts as a buffer to accommodate the volume expansion of Si NPs and thus preserve the overall electrode structure.

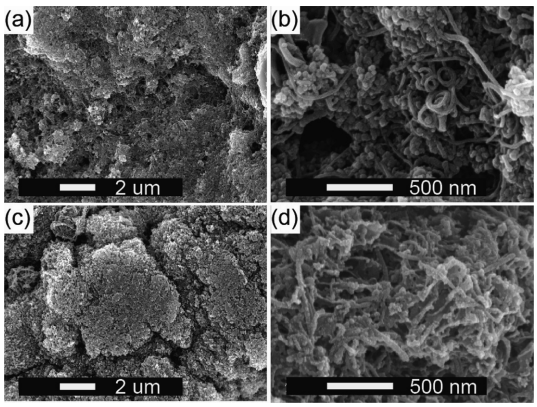

Fig. 6. SEM images of the 34 wt% SiNP@CNT composite at various stages of cycling. (a, b) SEM images of the composite electrode at the pristine state in different magnifications. (c, d) The same composite but after 100 cycles.

4. Conclusion

This study demonstrates that highly organized CNT network can serve as a good buffer component for a Si NPs-based anode in LIBs. The structural feature of embedding Si NPs in the CNTs network resolve critical issues linked to chronic capacity fading mechanisms such as Si pulverization, lost contacts between Si and conducting agents, and unstable SEI formation. The current composite structure turns out to hold a robust electrode structure over repeated cycles, which was reflected by outstanding electrochemical results in various aspects including cycle life and rate capability. The present investigation offers a design principle readily applicable to other alloying electrode materials that undergo large volume expansions during battery operations.

Acknowledgements

We are pleased to acknowledge the financial support by the National Research Foundation of Korea (NRF) grant funded by the Korea government (MEST) (NRF-2010-C1AAA001-0029031 and NRF-2012-R1A2A1A01011970) and the World Class University Program (R-31-2008-000-10055-0).

References

1. J. M. Tarascon and M. Armand, *Nature,* **414**, 359 (2001).
2. M. Armand and J. M. Tarascon, *Nature,* **451**, 652 (2008).
3. B. A. Boukamp, G. C. Lesh and R. A. Huggins, *J. Electrochem. Soc.,* **128**, 725 (1981).
4. A. S. Arico, P. Bruce, B. Scrosati, J.-M. Tarascon and W. van Schalkwijk, *Nat. Mater.,* **4**, 366 (2005).
5. C. K. Chan, H. Peng, G. Liu, K. McIlwrath, X. F. Zhang, R. A. Huggins and Y. Cui, *Nat. Nanotechnol.,* **3**, 31 (2008).
6. H. Kim, M. Seo, M.-H. Park and J. Cho, *Angew. Chem. Int. Ed.,* **49**, 2146 (2010).
7. S.-H. Ng, J. Wang, D. Wexler, K. Konstantinov, Z.-P. Guo and H.-K. Liu, *Angew. Chem. Int. Ed.,* **45**, 6896 (2006).
8. J. Yang, M. Winter and J. O. Besenhard, *Solid State Ionics,* **90**, 281 (1996).
9. L.-F. Cui, L. Hu, H. Wu, J. W. Choi and Y. Cui, *J. Electrochem. Soc.,* **158**, A592 (2011).
10. J. W. Choi, J. McDonough, S. Jeong, J. S. Yoo, C. K. Chan and Y. Cui, *Nano Lett.,* **10**, 1409 (2010).
11. C. K. Chan, R. N. Patel, M. J. O'Connell, B. A. Korgel and Y. Cui, *ACS Nano,* **4**, 1443 (2010).
12. M. Ge, J. Rong, X. Fang and C. Zhou, *Nano Lett.,* **12**, 2318 (2012).
13. M. T. McDowell, S. W. Lee, I. Ryu, H. Wu, W. D. Nix, J. W. Choi and Y. Cui, *Nano Lett.,* **11**, 4018 (2011).
14. M.-H. Park, M. G. Kim, J. Joo, K. Kim, J. Kim, S. Ahn, Y. Cui and J. Cho, *Nano Lett.,* **9**, 3844 (2009).
15. T. Song, J. Xia, J.-H. Lee, D. H. Lee, M.-S. Kwon, J.-M. Choi, J. Wu, S. K. Doo, H. Chang, W. I. Park, D. S. Zang, H. Kim, Y. Huang, K.-C. Hwang, J. A. Rogers and U. Paik, *Nano Lett.,* **10**, 1710 (2010).
16. H. Wu, G. Chan, J. W. Choi, I. Ryu, Y. Yao, M. T. McDowell, S. W. Lee, A. Jackson, Y. Yang, L. Hu and Y. Cui, *Nat. Nanotechnol.,* **7**, 310 (2012).
17. Y. Yao, M. T. McDowell, I. Ryu, H. Wu, N. Liu, L. Hu, W. D. Nix and Y. Cui, *Nano Lett.,* **11**, 2949 (2011).
18. J. Cho, *J. Mater. Chem.,* **20**, 4009 (2010).
19. T. H. Hwang, Y. M. Lee, B.-S. Kong, J.-S. Seo and J. W. Choi, *Nano Lett.,* **12**, 802 (2011).
20. A. Magasinski, P. Dixon, B. Hertzberg, A. Kvit, J. Ayala and G. Yushin, *Nat. Mater.,* **9**, 353 (2010).
21. H. M. Jeong, S. Y. Lee, W. H. Shin, J. H. Kwon, A. Shakoor, T. H. Hwang, S. Y. Kim, B.-S. Kong, J.-S. Seo, Y. M. Lee, J. K. Kang and J. W. Choi, *RSC Advances,* **2**, 4311 (2012).
22. L. Su, Z. Zhou and M. Ren, *Chem. Commun.,* **46**, 2590 (2010).
23. B. Hertzberg, A. Alexeev and G. Yushin, *J. Am. Chem. Soc.,* **132**, 8548 (2010).
24. J. W. Choi, L. Hu, L. Cui, J. R. McDonough and Y. Cui, *J. Power Sources,* **195**, 8311 (2010).
25. K. Hernadi, A. Fonseca, J. B. Nagy, D. Bernaerts and A. A. Lucas, *Carbon,* **34**, 1249 (1996).
26. H. Yoshida, S. Takeda, T. Uchiyama, H. Kohno and Y. Homma, *Nano Lett.,* **8**, 2082 (2008).
27. A. Netz, R. A. Huggins and W. Weppner, *J. Power*

Sources, **119–121**, 95 (2003).
28. S. Bourderau, T. Brousse and D. M. Schleich, *J. Power Sources,* **81–82**, 233 (1999).
29. U. Kasavajjula, C. Wang and A. J. Appleby, *J. Power Sources,* **163**, 1003 (2007).
30. Y. M. Lee, J. Y. Lee, H.-T. Shim, J. K. Lee and J.-K. Park, *J. Electrochem. Soc.,* **154**, A515 (2007).
31. L. Wang, C. X. Ding, L. C. Zhang, H. W. Xu, D. W. Zhang, T. Cheng and C. H. Chen, *J. Power Sources,* **195**, 5052 (2010).
32. J. P. Maranchi, A. F. Hepp, A. G. Evans, N. T. Nuhfer and P. N. Kumta, *J. Electrochem. Soc.,* **153**, A1246 (2006).